JOURNAL OF MATERIALS SCIENCE 32 (1997) 4485–4492

Microstructure and solid particle erosion of carbon-based materials used for the protection of highly porous carbon–carbon composite thermal insulation

R. I. BAXTER, R. D. RAWLINGS
Department of Materials, Imperial College of Science, Technology and Medicine, London SW7 2BP, UK

Multiparticle erosion tests were performed on candidate coating (colloidal graphite paints) and cladding (dense carbon–carbon composites and graphite foil) materials employed to protect porous carbon–carbon composite thermal insulation in vacuum and inert-gas furnaces that utilize inert gas quenching. The dependence of the erosion rate on the angle of incidence of the erodent was examined and related to the microstructure and the mechanisms of material removal as observed by SEM. In addition, the effect of a thin chemical vapour deposited (CVD) carbon layer on top of a colloidal graphite paint coating and a graphite foil clad was investigated. The coating and cladding materials displayed a greater erosion resistance at all angles of incidence compared to the porous carbon–carbon composite. In general, the greatest erosion rate was found at an angle of incidence of 90°, where the erodent stream is perpendicular to the erosion surface, and brittle fracture was the predominant mechanism of material removal. The exception was the graphite foil material which displayed maximum erosion at an angle of incidence of 60°. For this material, two mechanisms were effective: disruption of the graphite flakes, which are mainly held together by mechanical locking, and a ploughing-like mechanism. The addition of a thin CVD carbon layer to colloidal graphite paint improved performance, whereas the erosion resistance of the graphite foil was slightly degraded as the CVD layer was too thin to prevent the ploughing-like mechanism.

1. Introduction

A class of highly porous carbon–carbon (C–C) composites, with low densities in the range 0.1–0.4 $Mg\,m^{-3}$, are utilized as thermal insulation in vacuum and inert-gas furnaces at temperatures up to 2800 °C [1]. A consequence of the vacuum-moulding process used in the production of the composite is that the discontinuous fibres are orientated into layers to form a two-dimensional planar random structure. The vast majority of the volume of the composite consists of interconnected pores and the fibre network is bonded at the intersections of fibres by discrete regions of the carbon matrix as opposed to a continuous matrix. For this reason these composites are also known as carbon-bonded carbon fibre (CBCF). As a result of the high porosity and the fibre orientation, the thermal conductivity perpendicular to the fibre layer planes is low, a typical value for a material with a nominal density of 0.20 $Mg\,m^{-3}$ is 0.24 $W\,m^{-1}\,K^{-1}$ at 2000 °C in vacuum [2]. Investigations into the microstructure [3, 4], mechanical properties [2, 5–9] and thermal properties [10, 11] of these materials have been reported.

CBCF is used in furnaces employed in high technology applications such as single-crystal growing (for example, silicon or gallium arsenide) or metal heat treatment. The heat treatment of metals, such as tool steels, is increasingly carried out in furnaces that utilize gas quenching (typically nitrogen is used) [12, 13]. The gas quench may be used to reduce the turnaround time of batch processes or as an integral part of the heat-treatment regime. The advantage of gas quenching during heat treatment, as opposed to an oil quench, is that the cooling rate can be controlled; therefore, it is possible to reduce warping and cracking in the component [14]. During gas quenching, particulate matter may become entrained in the gas flows, and impingement with the insulation may result in material removal. In the challenging environment of gas quenching, there is a requirement for erosion protection of the CBCF by the use of higher density carbon-based coating and cladding materials.

Generally, ductile and brittle materials exhibit different erosion characteristics; of particular interest is their relationship between the erosion rate and the angle of incidence [15]. Ductile materials tend to

0022–2461

display maximum erosion at glancing angles of impact, approximately 30° for metals, and material removal is thought to occur by a micromachining mechanism [16] with a contribution of deformation wear at higher angles [17, 18]. On the other hand, for brittle materials, maximum erosion is found where the erodent stream is perpendicular to the erosion surface, and material removal typically results from the formation of Hertzian or lateral cracks [19]. Although it is a convenient approach to idealize materials erosion behaviour in this manner, it is an oversimplification, because erosion is found to depend on other factors, including the erosion conditions, such as erodent particle size and shape, as well as the details of the microstructure of the target material [20].

This paper is concerned with the examination of the microstructure and the effectiveness in improving the erosion resistance of several candidate coatings and claddings. The results presented involve the steady-state erosion rate as a function of impingement angle under defined conditions. The overall aim of this work is to relate the microstructure to the erosion data by means of a mechanistic approach.

2. Experimental procedure

2.1. Materials

The CBCF used as the substrate was a standard commercial material (density 0.18 $Mg\,m^{-3}$) manufactured by Calcarb Ltd. The coating and cladding materials were applied to the *xy* plane of the CBCF substrate (see the schematic diagram of CBCF structure in Fig. 1); the *xy* plane is perpendicular to the direction of minimum thermal conductivity and hence is most likely to be the exposed surface of the insulation in a furnace. The coating and cladding materials examined in this paper were all carbon based and they are listed in Table I. The coating materials are defined as those that bond independently to the CBCF substrate, whereas the claddings are bonded by means of a carbonizing cement. Calcoat and Calcoat M are colloidal graphite paint coatings that were applied to the CBCF substrate by brushing. The material was subsequently heat treated at 900 °C in nitrogen to carbonize the resin constituent of the colloid. Higher density carbon–carbon composites ($> 1.3\,Mg\,m^{-3}$) used as cladding materials included the Fiber Materials Inc. C^3 composite [21], which is resin impregnated, and the Toyo Tanso G3470 [22], which is resin impregnated and subsequently densified by chemical vapour deposition (CVD). In addition, a high-density carbon–carbon composite was produced by employing CVD over a period of 800 h to infiltrate a 5 mm thick section of the CBCF substrate to a density of $1\,Mg\,m^{-3}$. The CVD process used natural gas as the carbon precursor and nitrogen as the carrier gas. The densification was carried out at approximately 1100 °C under a reduced

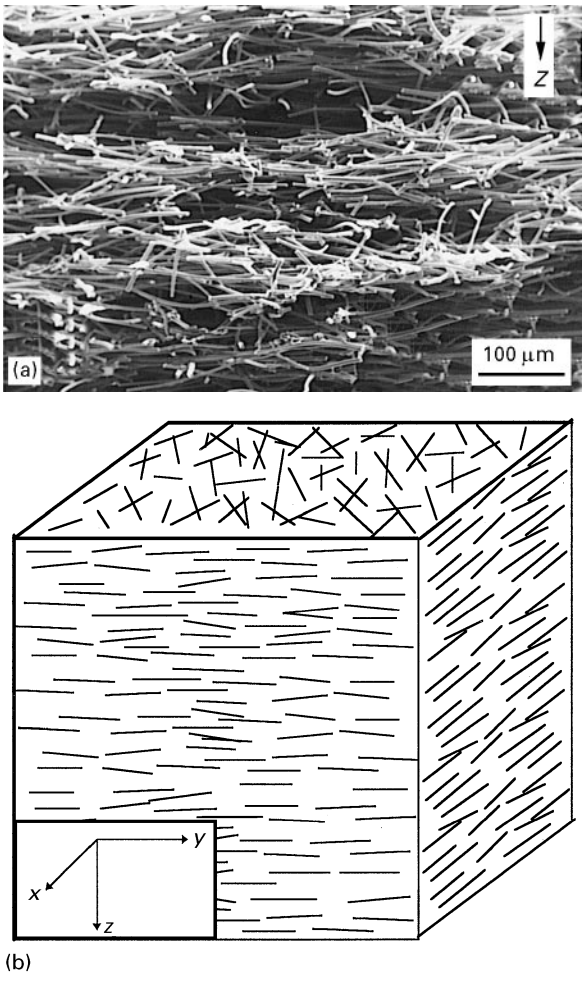

Figure 1 Carbon-bonded carbon fibre (CBCF): (a) scanning electron micrograph, and (b) schematic drawing of the structure.

TABLE I Manufacturer and density of the coating and cladding materials

Substrate	Manufacturer	Density ($Mg\,m^{-3}$)
CBCF Insulation	Calcarb Ltd, Scotland	0.18
Coatings		
Calcoat	Calcarb Ltd, Scotland	1.20[a]
Calcoat M	Calcarb Ltd, Scotland	1.20[a]
Calcoat + CVD	Calcarb Ltd, Scotland	> 1.20[a, b]
Claddings		
FMI C^3 2-dimensional woven C–C (resin impreg.)	Fiber Materials Inc., USA	1.30
G3470 C–C (resin impreg. + CVD)	Toyo Tanso, Japan	1.35
CBCF + CVD	Calcarb Ltd, Scotland	1.00[b]
Graphite foil	Toyo Tanso, Japan	1.00
Graphite foil + CVD	Toyo Tanso, Japan	> 1.00[a, b]

[a] Estimated values
[b] CVD treatment at Calcarb Ltd

pressure of 5 kPa. (Note that the CVD of carbon in the interior of a porous medium is sometimes termed chemical vapour infiltration, CVI.) Another cladding material was graphite foil which was produced by Toyo Tanso by compressing exfoliated graphite flakes in a rolling operation [23]. The foil is flexible in nature and is predominantly held together by mechanical locking, as no binder is used. Further samples were produced by subjecting the Calcoat coating and the graphite foil to a CVD treatment (samples designated + CVD in Table I) for a period of 75 h under the conditions described above. A more extensive description of the materials will be forthcoming in the discussion on the microstructures.

2.2. Erosion testing

Multiparticle erosion tests were performed on a gas-blast type rig, as described by Carter *et al.* [24]. In this apparatus the erodent particles enter the rig via an aperture in the base of an open hopper. A venturi fitted in the system allows the particles to be entrained in the compressed air flow. After passing through a nozzle with an 8 mm internal diameter, the particles strike the target at a stand-off distance of 40 mm. The target specimens had nominal dimensions 25 mm × 12.5 mm × 5 mm.

The erodent used was angular equiaxed silica sand obtained from Hepworth Minerals and Chemicals Ltd, Redhill, UK. The erodent was sieved to particle sizes between 150 and 300 μm, the mean size (by weight) was 230 μm which was found by a laser diffraction method (Mastersizer 1005, Malvern Instruments Ltd, Malvern, UK). The velocity of the particles was $6\,m\,s^{-1}$, found by the streaking camera technique at the position of the target. This method involved exposing the film for a known length of time and measuring the length of the line that the particle produces on the film. Erosion tests were carried out at angles of 30°, 45°, 60°, 75° and 90°.

Generally, the samples were impacted by a fixed mass of erodent, then cleaned and reweighed. This process was repeated and the accumulated mass loss plotted against the accumulated mass of erodent. The erosion rate, expressed in terms of mass removed per unit mass of erodent, was calculated from the gradient of these plots. However, in the case of the low-density CBCF substrate material, which was investigated for comparison purposes, a significant mass of erodent penetrated and was retained within the porous structure of the composite. When calculating the erosion rate, the mass of this penetrated erodent must be taken into account and therefore the erosion rate was found in the following manner. Each sample received only a single dose of erodent. The total mass change of each sample, ΔW_{total}, is equal to the mass of composite material removed by erosion, $\Delta W_{erosion}$, minus the mass of the retained erodent, W_{silica}

$$\Delta W_{total} = \Delta W_{erosion} - W_{silica} \quad (1)$$

The mass of penetrated, retained, erodent, W_{silica}, was found by oxidizing the carbon-based composite sample in a furnace at 800 °C to leave the silica residue, which was weighed. Subsequently, the mass of material removed by erosion, $\Delta W_{erosion}$, was calculated. Successive samples received incrementally increased doses and the mass of material removed by erosion plotted against the mass of erodent used, and the average erosion rate (in units of $g\,g^{-1}$) was found from the gradient of the best-fit line.

2.3. Microstructural and surface observations

Samples for optical microscopy were vacuum impregnated with resin and subsequently polished to a 1 μm finish. Samples for SEM were mounted on to aluminium tabs and examined at an accelerating voltage of 20 kV. In the majority of cases, coating was not required due to the sufficient electrical conductivity of the carbon samples; however, where charging of retained silica erodent was evident in the eroded samples, they were splutter coated with gold.

3. Results and discussion

3.1. Microstructure

The structure of CBCF insulation material is shown in Fig. 1; the porosity content of this fibre network is exceptionally high with 87% of the volume of the composite consisting of open and interconnected pores. The orientation of the fibres is evident in the micrograph in which the fibres lie preferentially in xy planes (i.e. perpendicular to the z direction) but are random in direction within these planes.

The thickness of the Calcoat colloidal graphite paint coating is variable, due to the brushing method of application, but generally is in the range 40–60 μm (Fig. 2a). However, as a result of the high porosity content and the interconnected nature of the porosity in the CBCF substrate, some of the paint penetrates up to a depth of 600 μm (Fig. 2b).

Calcoat M consists of Calcoat colloidal graphite paint, which contains sub-micrometre carbon particles, with the addition of coarser carbon particles and short fibres (< 50 μm). The coarser carbon particles increase the viscosity of the paint which results in a thicker surface coating (80–200 μm) by minimizing the extent of penetration into the interior of the porous substrate (Fig. 2c).

The Calcoat + CVD is produced by depositing carbon from the gaseous phase on to the Calcoat coating in the CVD furnace. This process produces a layer of dense pyrolytic carbon about 5 μm thick on the surface of the paint coating with little penetration (Fig. 2d).

The FMI C^3 C–C composite is produced from polyacrylonitrile (PAN) precursor carbon fibre cloth, which is about 1.2 mm thick [21]. The cloth is impregnated with phenolic resin but it is evident that the resin does not adequately penetrate the fibre bundles (Fig. 3a). Large platelets of resin-based carbon (500 μm × 500 μm × 40 μm) are found between the layers of woven cloth, as can be seen in the plan section micrograph in Fig. 3b. This may result from the use of a high-viscosity resin or a low impregnation pressure,

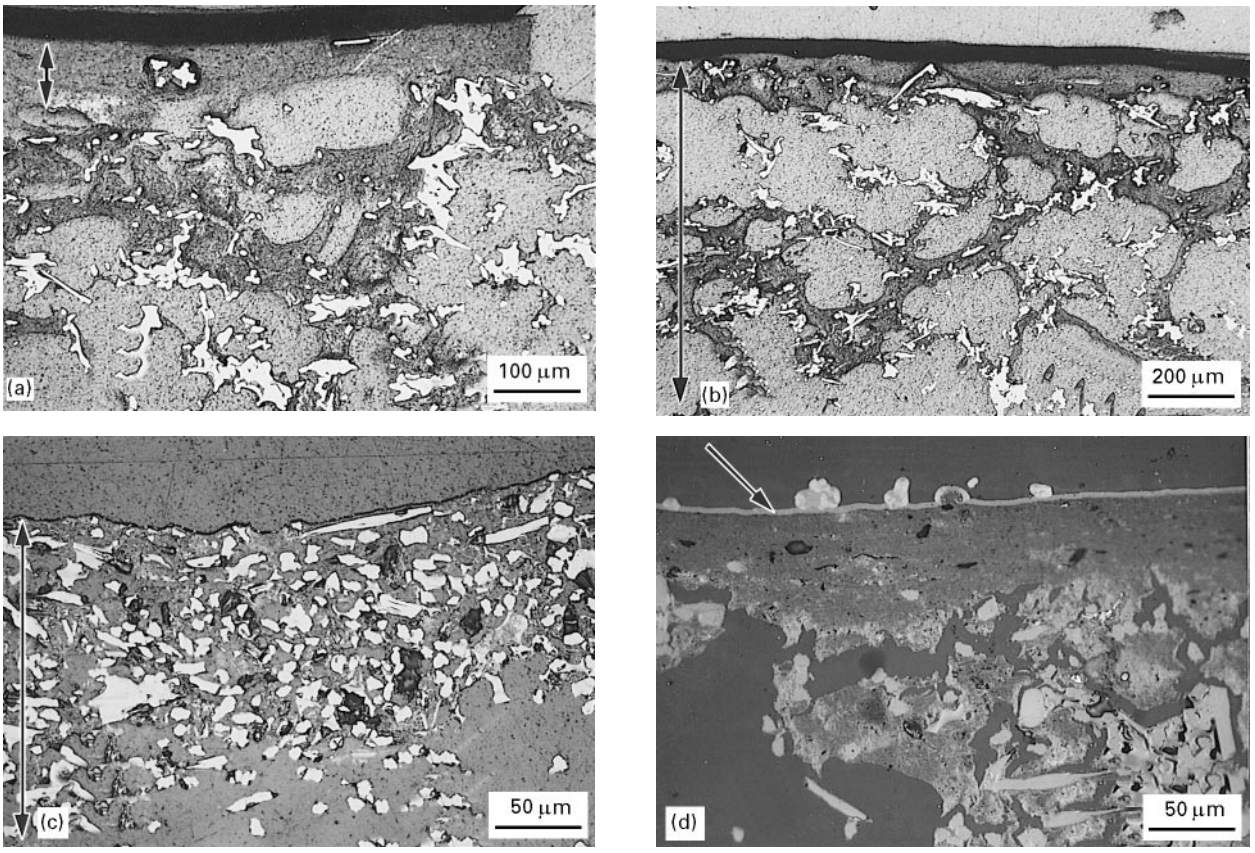

Figure 2 Optical micrographs of coatings (cross-sections; CBCF carbon fibres and matrix appear white in these micrographs): (a) Calcoat coating (thickness indicated by the arrow; Calcoat – dark grey; sample mounting resin – light grey), (b) Calcoat coating (depth of penetration indicated by the arrow; Calcoat – dark grey; sample mounting resin – light grey), (c) Calcoat M coating (thickness indicated by the arrow; carbon particles – white; sample mounting resin – grey), and (d) Calcoat + CVD coating (CVD layer indicated by the arrow appears white; Calcoat – light grey; sample mounting resin – dark grey).

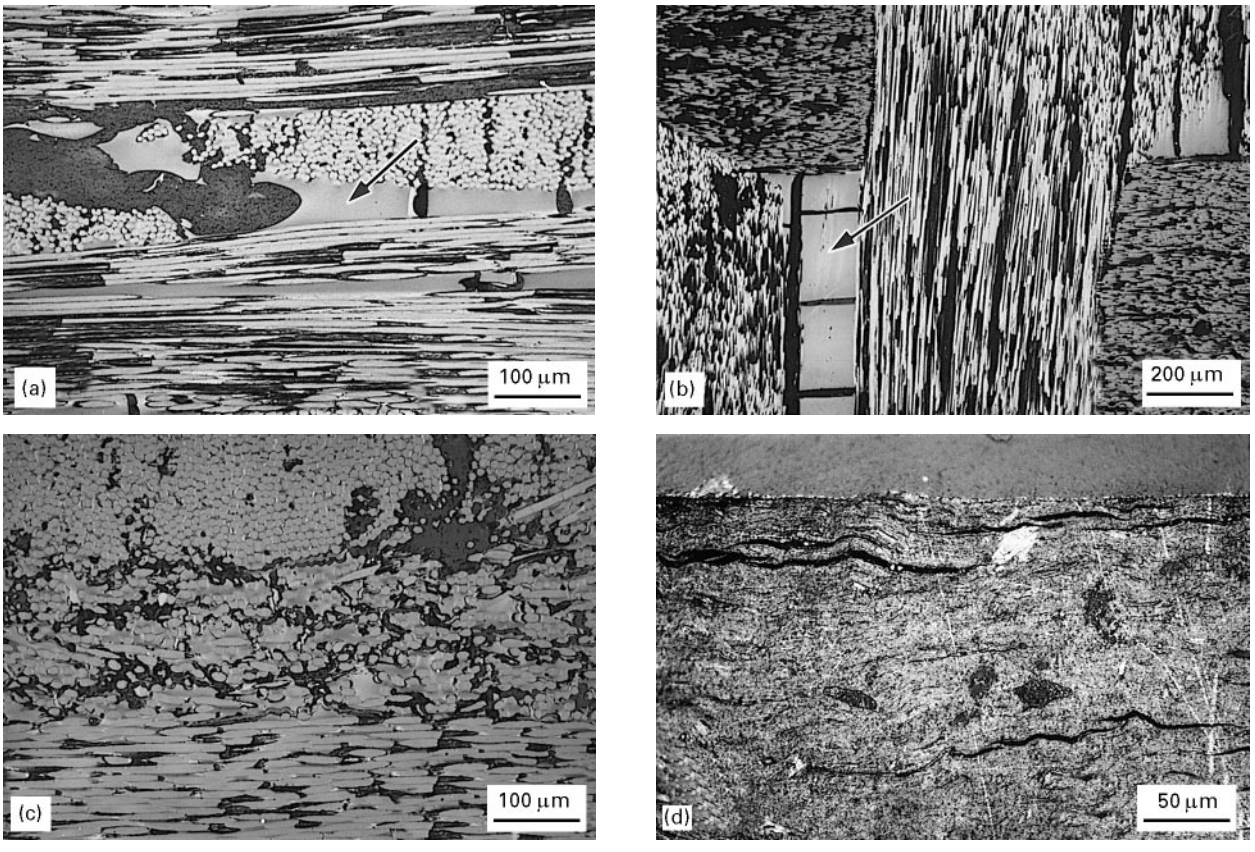

Figure 3 Optical micrographs of the cladding materials (Carbon fibres and matrix – white/light grey; sample mounting resin – dark grey). (a) FMI C^3 cladding (cross-section; matrix carbon platelets indicated by the arrow), (b) FMI C^3 cladding (plan section; matrix carbon platelets indicated by arrows), (c) Toyo Tanso G3470 cladding (cross-section), and (d) graphite foil (cross-section).

for example. The carbonization of the resin results in a large contraction (typically 50%) and the resin shrinks away from the fibres [25]. The separation of the matrix from the fibre suggests a low interfacial strength.

The Toyo Tanso G3470 C–C composite (Fig. 3c) is produced from unidirectional tows (300–700 μm thick) of PAN-based carbon fibres laid up in 0°/90° directions but interspersed with layers (approximately 100 μm thick) of shorter randomly aligned fibres. The composite is impregnated with resin which is subsequently carbonized. It is evident from the micrograph that the resin impregnation is more efficient compared with that for the FMI C^3; the resin penetrates into the intra-bundle regions and no large resin platelets are observed. The shrinkage of the resin on carbonization results in cracks but generally the integrity of the fibre–matrix interface is retained indicating a superior fibre–matrix bond. It is reported in the manufacturers technical information sheet that the G3470 composite is subjected to a CVD treatment [22]. However, the CVD matrix could not be distinguished, even as a surface layer, in the microstructure examined here.

For the CBCF sample densified by CVD, as a consequence of the interconnected porosity, the carbon deposits within the interior of the composite (Fig. 4). The deposit builds up a sheath around the fibres and as it increases in thickness, fibres that were not previously connected may be joined together. This process is accompanied by an increase in density and strength [26].

The graphite foil is produced by compressing exfoliated graphite flakes (typical dimensions 800 μm × 200 μm × 200 μm) in a cold-rolling operation to form a flexible foil (Fig. 3d) [27]. A consequence of the production method is that the flakes in the material lie parallel to the surface. The application of CVD to the foil produces a thin layer of carbon (~5 μm) on the surface of the foil similar to that on the surface of Calcoat + CVD, and in both cases the penetration of the deposit is limited.

3.2. Erosion

The insulation material, CBCF, displayed the highest rate of erosion of all the materials tested at all angles of incidence (Fig. 5). The mechanism of erosion is reported elsewhere [28]; fracture of the fibres is predominant, whereas the discrete matrix bonds remain intact. The rayon-derived carbon fibres in CBCF, used primarily for their low cost and low thermal conductivity, are relatively weak, with a typical strength of 0.35 GPa [29]. The debris particles are relatively large, typically of the order of 500 μm × 500 μm × 150 μm. The thickness of the debris particles, 150 μm, corresponds to the thickness of the layers in the composite, suggesting that sections of the layers are removed and it is known that relatively few fibres connect the layers together [3]. The similar erosion rates at 75° and 90° may be related to the high porosity of CBCF. The size of the pores (50–100 μm) are appreciable compared with the size of the erodent particles (230 μm) and

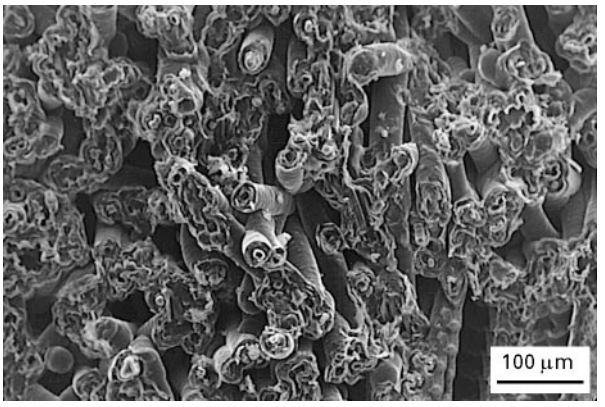

Figure 4 Scanning electron micrograph of the CBCF + CVD showing the sheaths around fibres.

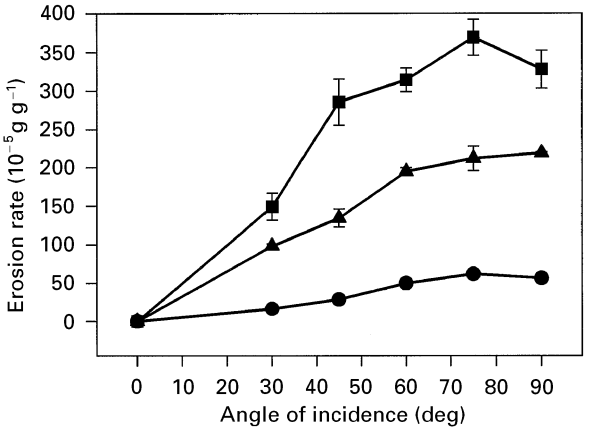

Figure 5 Erosion rate as a function of angle of incidence for (■) CBCF composite, (▲) Calcoat and (●) Calcoat M coating materials eroded by 230 μm silica particles at a velocity of 6 m s^{-1} (lines for ease of viewing).

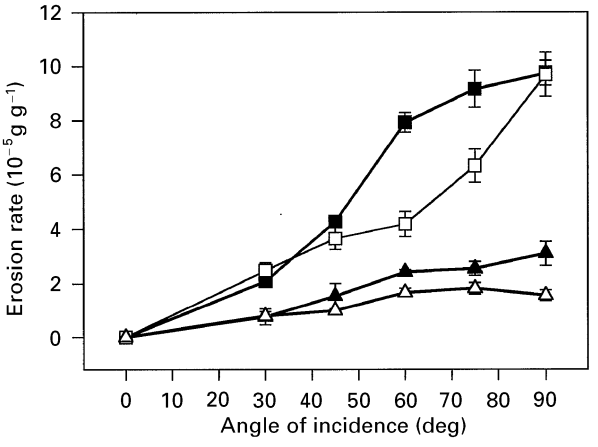

Figure 6 Erosion rate as a function of angle of incidence for (□) the Calcoat + CVD coating and (■) the FMI C^3, (▲) G3470 and (△) CBCF + CVD cladding materials eroded by 230 μm silica particles at a velocity of 6 m s^{-1} (lines for ease of viewing).

therefore the true angle of incidence at which an erodent particle would impinge the highly porous surface is similar for particles impinging at an average of 75° and 90°.

Calcoat and Calcoat M (Fig. 5) and Calcoat + CVD (Fig. 6) show the typical brittle material behaviour

with the maximum erosion rate at an angle of incidence of 90°. The Calcoat is eroded by extensive fracture of the carbonized coating on particle impact (Fig. 7a). The coating is not removed by ablation as it is well bonded to the substrate and the debris particles are relatively small with dimensions less than 100 μm. The coarser carbon particles and short fibres (< 50 μm in length) present in the Calcoat M coating do confer a degree of protection (Fig. 7b); the steady state erosion rate at normal angle of impingement is reduced by a factor of 4 compared with that of the Calcoat which only contains submicrometre particles. For the Calcoat + CVD sample, the thin CVD layer provides a large degree of erosion protection at all angles of incidence under the defined erosion conditions. This additional protection is to be expected, as pyrolytic carbon is a dense ($2.0\,Mg\,m^{-3}$ [9]) and relatively strong carbon material [30].

FMI C^3 and G3470 C–C composites show maximum erosion at an angle of impingement of 90° (Fig. 6). SEM of the erosion surface of the FMI C^3 composite (Fig. 7c) shows that, on fracture, the fibres are easily removed due to the limited penetration of the resin into the intra-bundle regions as shown in the microstructural examination. In the G3470 C–C composite, fibre fracture is observed but the removal of material is restricted by the superior fibre/matrix bonding, as the resin had penetrated the intra-bundle regions, and hence the erosion rate is reduced (Fig. 7d). The greater erosion resistance of the G3470 composite compared to the FMI C^3 composite is consistent with the work of Miyazaki and Takeda [31] on carbon fibre-reinforced Nylon composites; a decrease in the erosion rate was found as the fibre/matrix bond interfacial strength was increased by surface treatment of the carbon fibres.

The graphite foil material was exceptional in its behaviour with respect to angle with maximum erosion at an angle of incidence of 60° (Fig. 8). This relationship between the erosion rate and the angle of incidence was the same irrespective of whether the samples were cut with their 25 mm length parallel or perpendicular to the rolling direction of the foil. This behaviour indicates that an alternative mechanism of material removal is in operation in addition to, or in place of, brittle fracture. SEM analysis reveals that particle impact disrupts the packing of the graphite flakes and the resulting elevated flakes may be removed by a ploughing-like process (Fig. 9). This behaviour is a consequence of the fact that the flakes are mainly held together by mechanical locking, because the foil does not contain any binding medium. The disruption of the mechanical locking, which is probably accompanied by fracture of the flakes into smaller units due to the weakened nature of the Van der Waals forces in the exfoliated flakes, is most efficient at high angles of incidence where the kinetic energy of the particles perpendicular to the surface is greatest. In contrast, the ploughing mechanism whereby the elevated flakes are dug out, is expected to be more effective at glancing angles of impact; for example, in many metals, where this mechanism is predominant, the

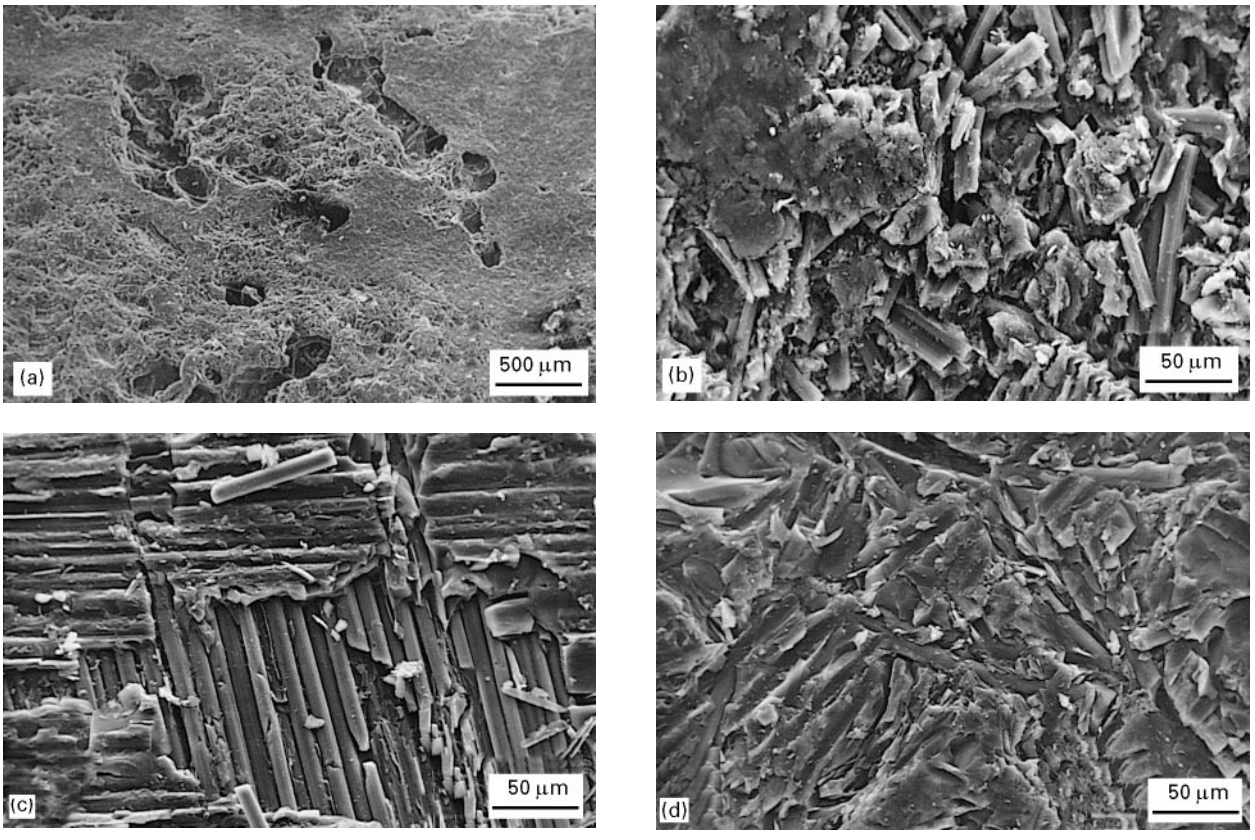

Figure 7 Scanning electron micrographs of the erosion surfaces (230 μm silica particles, velocity of $6\,m\,s^{-1}$, angle of incidence of 90°) of the (a) Calcoat (sample tilt of 40° in microscope), (b) Calcoat M (c) FMI C^3 cladding (sample tilt of 20° in microscope) and (d) Toyo Tanso G3470 composite.

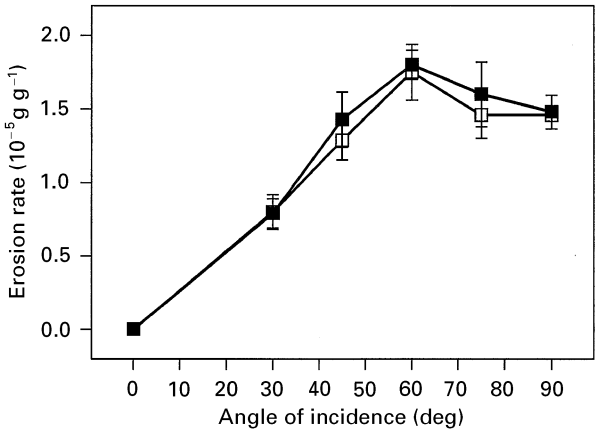

Figure 8 Erosion rate as a function of angle of incidence for the graphite foil cladding, in which the 25 mm length of the sample is (■) parallel and (□) perpendicular to the rolling direction, eroded by 230 μm silica particles at a velocity of 6 m s^{-1} (lines for ease of viewing).

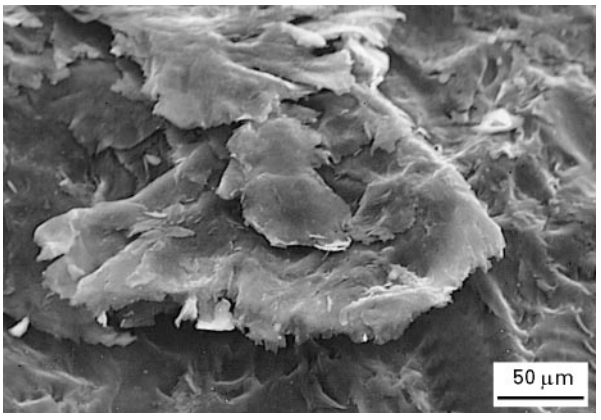

Figure 9 Scanning electron micrograph of the erosion surface (230 μm silica particles, velocity of 6 m s^{-1}, angle of incidence of 45°) of the graphite foil cladding showing elevated flakes (sample tilt of 40° in the microscope).

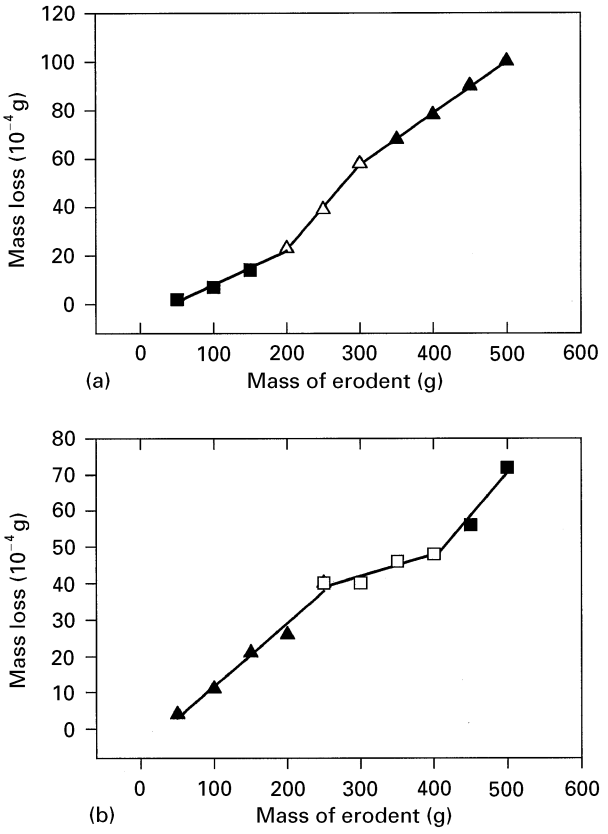

Figure 10 Mass loss plotted against the mass of erodent for the graphite foil cladding (25 mm length of the sample parallel to rolling direction) eroded by 230 μm silica particles at a velocity of 6 m s^{-1} at (a) an initial angle of incidence of (■) 90° and then (△) 45° (▲, 45° final) and (b) an initial angle of incidence of (▲) 45° and then (□) 90° (■, 90° final).

angle of maximum erosion is approximately 30°. The interdependence of these two mechanisms of material removal may explain the exceptional behaviour of the foil with respect to angle of incidence. The angle at which the maximum erosion occurs may be at a compromise angle, 60° in this case, at which both mechanisms complement each other.

Further investigation was employed to examine the synergistic relationship between the flake disruption and the ploughing-like mechanisms to examine if the action of one mechanism could facilitate material removal by the other. A sample was eroded at an initial angle of 90° until a steady-state erosion rate was found. At this point, the angle of incidence was changed to 45° and the experiment continued. The graph of the accumulated mass loss versus accumulated mass of erodent for surfaces eroded at an initial angle of 90°, then 45°, is shown in Fig. 10a. When the steady-state erosion surface set up under an initial angle of 90° is eroded at 45°, initially there is a large increase in the erosion rate and then the erosion rate is reduced but is still greater than expected on a virgin surface. It is suggested that the impingement of particles at 90° results in the disruption of the mechanical locking, and fracture of the flakes into smaller sizes, which facilitates their removal by a ploughing-like mechanism by particles impinging at 45°. On the other hand, for the surface initially eroded at 45° and then eroded at 90°, there is an initial reduction in the erosion rate and subsequently the erosion rate increases (Fig. 10b). The steady-state erosion surface of the foil eroded at 45° has many flakes that are partially lifted by the ploughing process. It is tentatively suggested that these elevated flakes increase the resilience of the surface which can then absorb the energy, by being flattened down, of a particle impinging perpendicularly on the surface. The subsequent increase in erosion rate is thought to occur when the flakes have been "flattened down" and are easier to remove due to the reduction in mechanical locking compared to flakes on a virgin surface.

The erosion rate curve for the CVD-treated foil generally lay above the corresponding curve for the graphite foil at angles below 90° (Fig. 11). SEM examination of the samples showed that the lifting and ploughing removal of the flakes was still effective at the lower angles of incidence. Therefore the flakes, coated with a CVD layer, are removed by the same mechanism, but due to the CVD layer being denser this results in an increase in erosion rate at angles of incidence lower than 90°. It is suggested that an improvement in the erosion resistance may occur if

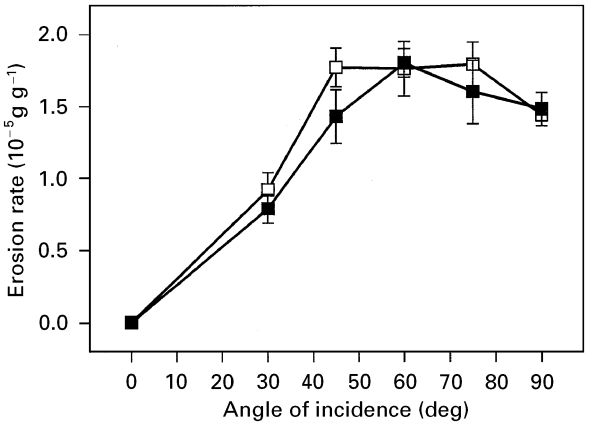

Figure 11 Erosion rate as a function of angle for (■) the graphite foil and (□) the graphite foil + CVD (25 mm length of the samples parallel to rolling direction) eroded by 230 μm silica particles at a velocity of 6 m s^{-1} (lines for ease of viewing).

thicker CVD deposits are employed that may inhibit the removal of the underlying flakes by the ploughing mechanism.

4. Conclusion

The materials used for coatings and claddings on porous CBCF composite displayed a significantly greater erosion resistance than the unprotected CBCF substrate under the conditions employed in this investigation. In general, the coating and cladding materials displayed the maximum erosion rate at angles of incidence in the region of 90° which is typical of brittle materials for which the mechanisms of material removal involve brittle fracture. The exception was the graphite foil material for which the maximum erosion rate was found at an angle of incidence of 60°. This behaviour was attributed to a mechanism whereby the graphite flakes, which are mainly bonded together by mechanical locking, were removed by a ploughing-like mechanism. It was demonstrated that the ploughing-like mechanism was facilitated by the disruption of mechanical locking by particles that impinged at higher angles of incidence to the erosion surface. The addition of a thin (5 μm) CVD layer on the colloidal graphite paint coating led to a considerable reduction in the erosion rate, whereas for the graphite foil the CVD layer slightly degraded the erosion resistance at angles below 90°, as the ploughing mechanism was still effective.

Acknowledgements

The authors thank the Engineering and Physical Sciences Research Council for the provision of a CASE award to support this project and also Chris Gee and Steve Ellacott of Calcarb Ltd (12 North Road, Bellshill, Strathclyde, ML4 1EN) for their additional funding, as well as assistance and encouragement.

References

1. J. MORGAN, *Metals Mater.* **9** (1988) 567.
2. G. C. WEI and J. M. ROBBINS, *Am. Ceram. Bull.* **64** (1985) 691.
3. I. J. DAVIES and R. D. RAWLINGS, *J. Mater. Sci.* **29** (1994) 338.
4. C. D. REYNOLDS and Z. L. ARDARY, Union Carbide Oak Ridge Y12 Plant Report no. Y/DA-6295 (1976).
5. C. D. REYNOLDS, Union Carbide (Nuclear Division) Oak Ridge Y12 Plant Report no. A74-35833 (1976).
6. I. J. DAVIES and R. D. RAWLINGS, in "Proceedings of the 6th European Conference for Composite Materials", edited by A. R. Bunsell, A. Kelly, A. Massiah (Woodhead, Cambridge, 1993) pp. 553–8.
7. *Idem*, *Composites* **25** (1994) 229.
8. *Idem*, *Carbon* **32** (1994) 1449.
9. S. D. ELLACOTT, MSc thesis, University of Surrey, Guildford, UK (1994).
10. T. G. GODFREY, D. L. McELROY and Z. L. ARDARY, *Nucl. Technol.* **22** (1974) 94.
11. N. E. HAGER and R. C. STEERE, *J. Appl. Phys.* **38** (1967) 4633.
12. J. G. CONYBEAR, *Adv. Mater. Process.* **2** (1993) 20.
13. B. J. BIRCH and B. ELLIS, in "Vacuum Engineering", edited by N. S. Harris (McGraw-Hill, London, 1991) pp. 165–233.
14. A. KAY, *Vacuum* **42** (1991) 1103.
15. A. W. RUFF and S. M. WIEDERHORN, in "Treatise on Materials Science and Technology", Vol. 16, "Erosion", edited by C. Preece (Academic Press, New York, 1979) pp. 69–126.
16. I. FINNIE, *Wear* **3** (1960) 87.
17. J. G. A. BITTER, *ibid.* **6** (1963) 5.
18. *Idem*, *ibid.* **6** (1963) 169.
19. G. L. SHELDON and I. FINNIE, *J. Eng. Ind.* November (1966) 393.
20. I. M.HUTCHINGS, in "Erosion of Brittle Materials", edited by J. E. Ritter (Trans Tech Publications, Zurich, Switzerland, 1991) pp. 75–92.
21. Fiber Materials Inc., Company Technical Information Sheet (1991).
22. Toyo Tanso Ltd, Company Technical Information Sheet (1991).
23. Gee Graphite Ltd, Company Technical Information Sheet (1991).
24. S. CARTER, R. D. RAWLINGS and P. S. ROGER, in "Advanced Ceramics in Chemical Process Engineering", British Ceramic Proceedings, London, 1988, edited by B. C. H. Steele (Institute of Ceramics, London, 1989) pp. 13–27.
25. G. M. JENKINS and K. KAWAMURA, "Polymeric Carbons, Carbon Fibre, Glass and Char" (Cambridge University Press, Cambridge, 1976) p. 27.
26. I. J. DAVIES, PhD thesis, Imperial College, University of London (1992).
27. D. D. L. CHUNG, *J. Mater. Sci.* **22** (1987) 4190.
28. R. I. BAXTER and R. D. RAWLINGS, *Mater. Sci. Technol.*, to be published.
29. H. M. STOLLER, B. L. BUTLER, J. D. THEIS and M. L. LIEBERMAN, in "Composites: State of the Art, Proc. Sess. Fall Meeting, 1971", edited by J. W. Weeton (AIME, New York, USA, 1971) pp. 69–136.
30. J. C. BOKROS, in "*Chemistry and Physics of Carbon*", Vol. 5, edited by P. L. Walker (Dekker, New York, 1969) pp. 1–119.
31. N. MIYAZAKI and N. TAKEDA, *J. Compos. Mater.* **27** (1993) 21.

Received 30 January
and accepted 10 March 1997